Copyright © 2007 Tech Science Press FDMP, vol.3, no.2, pp.115-128, 2007

Modeling the Flow of Molten Steel in a Tundish Containing an Inclusion Filtering Trap

A.K. Plappally[1], M.A.R. Sharif[1], and R.C. Bradt[2]

Abstract: A novel physical chemical filtration process in a tundish for removal of inclusion particles from molten steel is proposed and analyzed. The considered inclusion particles are mainly composed of the minerals alumina (Al_2O_3) and spinel ($MgAl_2O_4$), which have an affinity to adhere (on contact) to an inclusion trap. An industrial tundish is considered and modified with a zigzag channel block insert installed across the molten steel flow so that when the molten steel flows through the zigzag channels, the inclusion particles are driven into contact with the channel surfaces by increased recirculation and turbulence. The inclusions will bond with the surfaces and be removed from the molten steel. The flow behavior in a fully three-dimensional model of such a tundish, with and without the incorporation of the zigzag channels, is then modeled and dynamically simulated. The flow patterns and particle trajectories are then computed and critically analyzed leading to the conclusion that the proposed filtering system is practically feasible.

Keyword: Tundish, inclusion particles, inclusion removal, zigzag channel.

Nomenclature

d_p Diameter of the inclusion particle
g Acceleration due to gravity
h Channel spacing
k Turbulent kinetic energy
m_p Particle mass
$\overline{p}$ Mean fluid pressure
Re Reynolds number
t Time
$\overline{u}_i$ Mean velocity components
u_i' Fluctuating velocity component
U_f Mean velocity vector of the fluid phase
U_r Fluid velocity vector relative to the particle
U_p Velocity vector of the particle

Greek Symbols

μ Viscosity
μ_t Turbulent eddy viscosity
ρ Density
ρ_f Density of the fluid phase
ρ_p Density of the particle
θ Zigzag angle for the channel
ω_p Spinning velocity vector for the particle

1 Introduction

One of the most critical aspects of steel quality is its cleanliness with regard to inclusion content. Inclusion particles in cast steel may originate from various sources within the molten steel before casting. Steel producers know that the presence of inclusions directly affects the quality of their products through the generation of defects, in the hot workability of the steel, and as the sources for fatigue crack initiation. Inclusions are also a serious problem in the formation of accretions in submerged entry nozzles (SENs) at tundish outlets. Clean steel, however, is usually defined by consumer demand rather than in terms of composition or inclusion levels because this definition depends on the final application of steel products. While total elimination of inclusion particles from steel is probably an unrealistic goal, the decrease, removal, and control of the inclusions in the cast steel is an important aspect in all steel production processes.

[1] Aerospace Engineering and Mechanics Department, The University of Alabama, Tuscaloosa, Alabama 35487-0280, U.S.A.
[2] Metallurgical and Materials Engineering Department, The University of Alabama, Tuscaloosa, Alabama 35487-0202, U.S.A.

Physical sieving of the inclusion particles is impractical because the sieve will be rapidly clogged. Historically, various filtering techniques have been applied for the removal of inclusions from the molten steel in the tundish. These include foams or porous filters (Ichibashi, 1986) and processes utilizing various physical properties such as the bubble trapping of particles (Chevrier, 2000), floatation (He and Sahai, 1990), electro-magnetic separation (Taniguchi and Brimacombe, 1997), etc. However, these techniques produced limited success in attaining the required level of inclusion removal. The search for an alternative effective inclusion removal system from the molten steel in the tundish is a continuing and an active research area. The present article considers an alternative inclusion removal system from the molten steel while it is in the tundish.

A large portion of the inclusion particles in aluminum-killed molten steel poured into the tundish consists of the minerals spinel ($MgAl_2O_4$) and alumina (Al_2O_3) which are high melting point oxides that have a very strong affinity to adhere/bond to oxides (Itoh, Hino, and Ban-ya, 1997) as evident by the formation of accretions in the SEN. This bonding or chemical adherence is to be exploited in the proposed filtration/trapping technique for removing the inclusions from the steel. A refractory block of vertically stacked zigzag channels will be strategically placed across the steel flow direction within the tundish. The zigzag channel block may either be manufactured wholly of spinel or the channel surfaces may be coated with spinel. The concept is that the steel flow through the tortuous channels induces recirculation and increased turbulence so that the inclusion particles come in contact with the channel surfaces and adhere to them. Once the particles hit the channel surface, it is expected that they will chemically bond with the surface thereby being removed from the molten steel. This phenomenon actually occurs during the clogging of the SENs by the formation of accretions at the SEN exit. In principle, the zigzag channel block may be physically removed from the tundish and replaced with a new block once the old block becomes clogged with trapped inclusions.

The success of physiochemical entrapment of inclusion particles from molten steel in the tundish must be evaluated in actual field trials with an industrial tundish. However, before the field trial, preliminary modeling studies of the actual design of the zigzag channels, the flow behavior of the steel with the channels, and the resulting trajectories of the inclusion particles are necessary to assess the potential effectiveness of the filtering system. This can be accomplished using numerical simulation/modeling of the tundish equipped with the zigzag channel inclusion trapping system. The present article describes such a preliminary numerical study about the feasibility of incorporating a proposed inclusion removal system in an actual industrial tundish. The flow behavior of the molten steel and the trajectories of the inclusion particles within the tundish and through the zigzag channels are numerically computed and the results are graphically presented.

Mathematical/numerical models for tundish flow analysis have been previously employed by several researchers. Chakraborty and Sahai (1991) in a study of the effects of turbulent collisions, re-oxidation, flotation, and inclusion size distribution, predicted the removal of alumina inclusions from molten steel in a continuous casting tundish. Shen, Khodadadi, Pien, and Lan (1994) completed turbulence measurements and also finite-element simulation for the tundish flow of aluminum and found favorable agreement between the experiment and prediction. Sheng and Jonsson (1999) conducted water modeling of the tundish flow and applied a three-dimensional transient mathematical model to observe significant buoyancy effects. Lopez-Ramirez, Morales, and Serrano (2000) performed numerical simulation of the effects of buoyancy forces and flow control devices on fluid flow and heat transfer in a tundish. Javurak, Kaufmann, Gerhard, and Philipp (2002) noticed that recirculation volumes and turbulent particle diffusion were the reasons for unsatisfactory particle separation. They noted that the turbulent shear forces in the molten steel affects the coagulation of inclusions in the tundish. Nakashima, Tanaka, Fukuda, Kiyose,

and Yamada (2003) observed that in an actual tundish the turbulence dissipation rate is largest near the inlet nozzle, but extremely small in all other regions. They studied various design parameters such as the inlet shroud immersion depth, different outlet positions, and different designs of the pour boxes for flow optimization with various turbulence models. Jha and Dash (2002, 2004) evaluated different turbulence models of the $k-\varepsilon$ family for the prediction of tundish flow and concluded that the RNG $k-\varepsilon$ model performs better than the other variants of the $k-\varepsilon$ model. For other results on solidification problems (in other geometries) and related possible numerical approaches, the reader may consider the following recent works: Amberg and Shiomi (2005), who studied the effect of various types convection on generic solidification problems; Ludwig, Gruber-Pretzler, Wu, Kuhn and Riedle (2005), who numerically investigated (using the FLUENT CFD code) the formation of macrosegregations during continuous casting of Sn-Bronze and discussed the impact of different convection types (inlet flow, thermal and solutal buoyancy flow, and feeding flow); Abhilash, Joseph, and Krishna (2006) who used artificial neural networks algorithms for the prediction of dendritic parameters and macro hardness variation in permanent mould castings; Hong, Zhu, and Lee (2006) and Narski and Picasso, (2007) who introduced new models for the numerical simulation of dendritic growth in alloy solidification with melt convection, etc.

The present study consists of two parts. The first is the hydrodynamic design optimization of the zigzag channel. It is performed numerically considering the two-dimensional geometry of a single zigzag channel. Suitable channel design is decided on the basis of results of a parametric study and examination of the flow behavior and particle trajectories within the channel. In the second part, a numerical model for a three-dimensional industrial tundish is developed. Steel flow and particle trajectories in the tundish are computed and analyzed. Finally, the tundish flow model is modified by inserting a vertically stacked block containing multiple zigzag channels with the same geometrical design obtained in part one of the study. The flow and particle trajectory computations are then repeated. The results are analyzed and the feasibility of the proposed inclusion trapping/removal technique is discussed.

The tundish used in the model is a delta tundish that is symmetrical about the mid-plane through the inlet shroud. Because of this symmetry only half of the tundish is modeled. The geometry of the symmetric half of the tundish and its modified version with the block of zigzag channel insert in place is shown in Fig. 1.

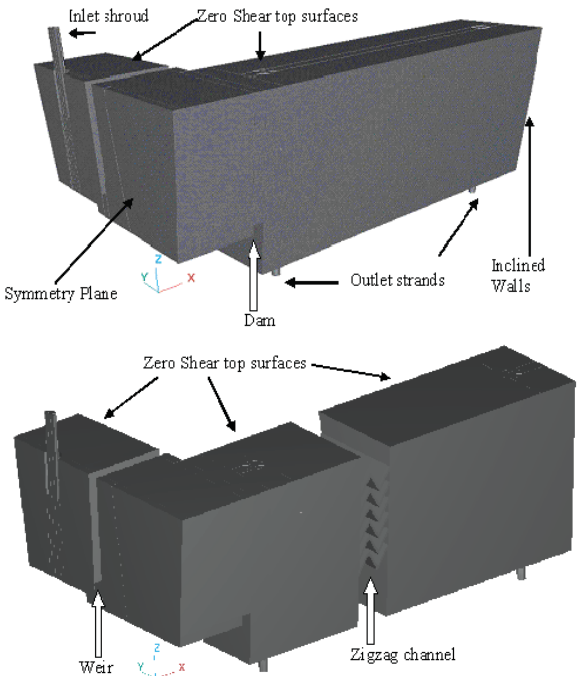

Figure 1: The modeled tundish schematic showing the geometric features; the bottom figure shows the tundish with the zigzag channel block insert in place.

The main tundish tank is in the longitudinal direction while the pouring block containing the inlet shroud is projected in the span wise direction. It is separated from the main tundish by a weir. The entering steel flow is poured through the inlet shroud onto the pouring block. The steel flow passes beneath the weir and is divided into two equal parts and turns longitudinally and flows over a span-wide small dam into the main tundish

tank, then exits through the two outlet strands at the bottom on each side. One of the outlets is located near the dam while the other outlet is further downstream close to the end wall. The zigzag channel inclusion trap is inserted at a strategic position in between the two outlets in the modified tundish model.

In order to impose a Cartesian coordinate system onto the tundish geometry, the x direction is assigned parallel to the longitudinal direction of the main tundish cavity. The y direction is assigned span-wise and z direction is the vertical. The origin of the coordinate system is positioned at the intersection of the lower edge of the symmetry plane and the vertical mid-plane through the main tundish cavity, hence $y = 0$ on that plane. The longitudinal half length of the tundish is 2.79 m (110 in.) while the overall tundish height is 1.07 m (42 in.). The span-wise bottom and top widths of the main cavity are 0.4318 m (17 in.) and 0.668 m, (26.3 in.), respectively. The sidewalls and end walls of the main tundish cavity are slightly inclined (about 18^o with the vertical).

2 Mathematical formulation

2.1 Governing equations for fluid motion

The governing equations for the incompressible flow consist of the conservation of mass and the Reynolds averaged Navier-Stokes (RANS) equations. They are written in the indicial notation as the following:

$$\frac{\partial \overline{u}_i}{\partial x_i} = 0 \tag{1}$$

$$\frac{\partial (\rho \overline{u}_i)}{\partial t} + \frac{\partial (\rho \overline{u}_i \overline{u}_j)}{\partial x_j} = \rho \overline{f}_i + \frac{\partial}{\partial x_j}\left[-\overline{p}\delta_{ij} + \mu\left(\frac{\partial \overline{u}_i}{\partial x_j} + \frac{\partial \overline{u}_j}{\partial x_i}\right) - \rho\overline{u_i' u'}_j\right] \tag{2}$$

where $\overline{u}_i$ are the mean velocity components, x_i are the coordinate directions, ρ is the fluid density, t is the time, $\overline{f}_i$ is the body force per unit mass, $\overline{p}$ is the mean pressure, δ_{ij} is the Kronecker delta, μ is the fluid dynamic viscosity, and u_i' are the fluctuating velocity components. The Reynolds stresses in the right hand side of Eq. (2) are:

$$-\rho\overline{u_i' u_j'} = \mu_t\left(\frac{\partial \overline{u}_i}{\partial x_j} + \frac{\partial \overline{u}_j}{\partial x_i}\right) - \frac{2}{3}\rho k \delta_{ij} \tag{3}$$

where μ_t is the turbulent eddy viscosity and k is the kinetic energy of turbulence. Applying the standard $k-\varepsilon$ model (Launder and Spalding, 1974), the eddy viscosity is given as

$$\mu_t = \rho C_\mu \frac{k^2}{\varepsilon} \tag{4}$$

where ε is the turbulence dissipation. The kinetic energy of turbulence, k, and its dissipation rate, ε, are obtained by solving their respective transport equations whose modeled forms are given as

$$\frac{\partial(\rho k)}{\partial t} + \frac{\partial(\rho k \overline{u}_j)}{\partial x_j} = \frac{\partial}{\partial x_j}\left[\left(\mu + \frac{\mu_t}{\sigma_k}\right)\frac{\partial k}{\partial x_j}\right] + P_k - \rho\varepsilon \tag{5}$$

and

$$\frac{\partial(\rho \varepsilon)}{\partial t} + \frac{\partial(\rho \varepsilon \overline{u}_j)}{\partial x_j} = \frac{\partial}{\partial x_j}\left[\left(\mu + \frac{\mu_t}{\sigma_\varepsilon}\right)\frac{\partial \varepsilon}{\partial x_j}\right] + C_{1\varepsilon}P_k\frac{\varepsilon}{k} - C_{2\varepsilon}\rho\frac{\varepsilon^2}{k} \tag{6}$$

where the production term $P_k = -\rho\overline{u_i' u_j'}(\partial \overline{u}_j/\partial \overline{u}_i)$. The model constants in Eqs. (5) and (6) are; $C_\mu = 0.09$, $C_{1\varepsilon} = 1.44$, $C_{2\varepsilon} = 1.92$, $\sigma_k = 1$, and $\sigma_\varepsilon = 1.3$. Standard wall function prescriptions (Launder and Spalding, 1974) at the wall are used to solve the equations.

2.2 Governing equation for particle motion in fluid

Particle motion in a fluid is governed by the Lagrangian equation of motion

$$m_p\frac{\partial U_{pi}}{\partial t} = F_{Wi} + F_{Di} + F_{Pi} + F_{SLi} + F_{MLi} \tag{7}$$

where m_p is the mass of the particle, U_p is the particle velocity vector, F_W is the body force term expressing the difference between the weight and the buoyancy force on the particle, F_D is the drag

force, F_P is the pressure gradient force, F_{SL} is the Saffman lift force, and F_{ML} is the Magnus lift force. The subscript index i is the tensor index and stands for the ith coordinate direction.

The body force is given by

$$F_{Wi} = \frac{\pi}{6} d_p^3 (\rho_p - \rho_f) g_i \tag{8}$$

where $g_i$is the component of gravitational acceleration in the ith direction.

The drag force is given by

$$F_{Di} = \frac{1}{2} \rho_f U_{ri} |U_{ri}| A_{pi} C_D \tag{9}$$

where ρ_f is fluid density, U_r is the relative fluid velocity with respect to the particle, A_{pi} is the frontal area of the particle as seen from the ith direction, and C_D is the drag coefficient. The relative fluid velocity vector is given by $U_r = U_f - U_p$ where U_f is the fluid velocity vector. The ith component of U_r is used in Eq. (9). The particle shape is considered spherical for which the drag coefficient, C_D, is given by $24/Re_{pi}$. This assumes that the particle Reynolds number, Re_{pi}, is very small. The particle Reynolds number is defined in terms of the relative velocity (U_{ri}) and particle diameter (d_p) as $\rho_f U_{ri} d_p / \mu$. Other prescriptions for C_D over a wide range of Reynolds number are available in Clift, Grace, and Weber (1978).

The pressure gradient force on the particle is given by

$$F_{Pi} = -(\pi/6) d_p^3 (\partial p / \partial x_i) \tag{10}$$

Small particles in a shear field experience a lift force perpendicular to the flow direction of the fluid phase. This lift originates from the inertia effects in the viscous flow around the particle. The expression for the inertial shear lift was first presented by Saffman (1965). It is written in the following form (Ran, Zhang, Tang, and Xin, 2006),

$$F_{SLi} = 1.615 (\rho \mu)^{0.5} d_p^2 U_{rj} \left| \frac{\partial U_{rj}}{dx_i} \right|^{0.5} sgn \left(\frac{\partial U_{rj}}{dx_i} \right) \tag{11}$$

where the "sgn" term in the right hand side is either 1 or -1 depending on whether the derivative term in its argument is positive or negative.

Local flow vorticity may cause the particles to spin. For spinning particles in a fluid stream, an additional force perpendicular to the streamwise direction is created. This is called the Magnus lift force. The Magnus lift force on the particles spinning at an angular velocity vector, ω_p, initiated by the fluid rotation is expressed as (Lun and Liu, 1997)

$$F_{ML} = \frac{1}{2} \rho_f (U_r \cdot U_r) \frac{\pi d_p^2}{4} C_{ML} \frac{\omega_p \times U_r}{|\omega_p| \, |U_r|} \tag{12}$$

The angular velocity vector of the particle can be obtained from the local vorticity as $\omega_p = (1/2) \nabla \times U_f$ and the coefficient C_{ML} is given by

$$C_{LM} = d_p \, |\omega_p| \Big/ |U_r| \tag{13a}$$

if $\mathrm{Re}_p \leq 1$, and

$$C_{LM} = d_p \, |\omega_p| \Big/ |U_r| \left(0.178 + 0.822 \mathrm{Re}_p^{-0.522} \right) \tag{13b}$$

if $1 < \mathrm{Re}_p < 1000$.

It is to be noted that the ith component of F_{ML} must be used in Eq. (7) and Re_p is defined as $\rho_f U_r d_p / \mu$.

The particle trajectories are also affected by turbulent eddies which can be incorporated by numerically generating the fluctuating velocity components u_i', and adding those to the local mean fluid velocity components, U_{fi}, for every time step integration of Eq. (7) [Schwarze, Obermeier, and Janke (2001) and Varga-Zamora, Morales, Diaz-Cruz, Palafox-Ramos, and Demedices (2003)]. Therefore, the inclusion particles will be more dispersed and the chances of the particles impacting the channel surfaces will be increased. This effect will also aid the inclusion particles in getting out of the "closed streamlines" encompassing the recirculation regions. The fluctuating velocity components can be generated as $u_i' = \xi \sqrt{k}$ where ξ is the product of a random number between -1 and 1 and an empirical constant. That turbulent dispersion effect, however, has not been considered in the present study.

2.3 Details of the numerical process

The governing equations were solved through the application of the commercial computational fluid dynamics code, CFD-ACE+^{TM} (ESI-CFD, 2006). The flow domain was divided into small finite volume cells with an unstructured tetrahedral mesh. The governing RANS equations and the transport equations for k and ε were integrated over each cell to generate a linear system of algebraic equations. These were then solved sequentially. The convective fluxes in the transport equations were calculated using the second-order upwind scheme while the diffusive fluxes are calculated using the central differencing scheme. The linear system for each transport equation was solved iteratively until convergence when the residuals are very small for each equation. The pressure velocity coupling was achieved using the well known SIMPLE method (Patankar, 1979). A time marching procedure with first-order accurate forward differencing time integration was applied to reach the steady-state solution until the variation of each variable between two successive time-steps is insignificant over all cells.

For the simulations, the density and viscosity of molten steel was specified to be 7000 kg/m^3 and 0.0055 Pa s, respectively. An assumed temperature of 1875 K was used.

The particle trajectories were calculated by activating the relevant component of the CFD-ACE+^{TM} code. Once the steady-state hydrodynamic field was solved, it was then frozen and the particles were introduced into this hydrodynamic field with the local initial velocity for the specific point of introduction. Time integration of Eq. (7) governing the particle motion was then used to calculate particle locations for each particle using small time steps. The locations were then joined by a curve to display the particle trajectories. No chemistry/chemical kinetics model for the particle-particle coagulation/agglomeration or particle to wall adsorption was used to compute the particle trajectories. For the particle trajectory calculation, one way coupling was assumed, meaning the particle motion is affected by the hydrodynamic field, but the hydrodynamic field is not affected by the particle motion. This is a valid assumption since the particle distribution in the molten steel is a very dilute one of well dispersed particles. Also particle to particle collision was not considered in the calculations. However, particle to wall collision was considered through the use of a coefficient of restitution, which has a value between 0 and 1. When the coefficient of restitution is zero, it is a fully plastic collision in which case the particle is assumed to stick to the wall after collision. On the other hand if it is 1, it is a fully elastic condition in which case the particle bounces back with the same speed as before the collision. The fully plastic condition for the particle to channel wall collision by setting the coefficient of restitution to 0 will be used later to simulate the bonding of the particles with the channel walls in lieu of any model to describe the inclusion capture rate. In all trajectory calculation, spherical particles of 1-100 μm diameter with a mass density of 4000 kg/m^3 were considered. This density is representative of typical oxide inclusion particles.

3 Results and Discussion

3.1 Zigzag Channel Design

As mentioned in the introduction, the zigzag channel insert in the tundish is the core of the proposed inclusion filtering/trapping technique. The objective is to utilize the increased recirculation and turbulence of the molten steel while passing through the zigzag channel to bring the inclusion particles in contact with the channel surfaces. The inclusions are then expected to chemically react with the channel surface and bond to it and thus be trapped. It is essentially duplicating the conditions which create the accretions at the SEN exit. As such, a detailed simulation of the flow behavior and particle trajectories through the zigzag channel is required in order to optimize the design of the channel configuration which will be used in an actual tundish. First, a two-dimensional channel design, as shown in Fig. 2, is adopted to evaluate its effectiveness even though the actual tundish flow is three-dimensional. This, however, is not a gross simplification since the flow through the three-dimensional zigzag channel will be basi-

cally a two-dimensional one, i.e., the variation in the span-wise direction within the channels will be insignificant. This particular configuration for the zigzag channel was chosen to facilitate the ease of fabrication of the channel insert and to minimize the space for the placement of the insert in the existing tundish.

The channel is to be placed within the tundish where the general flow direction is upward and closely matches the entry channel angle. This is to be determined by examining the three-dimensional simulation of the tundish flow without the presence of the zigzag channel. The zigzag channel exit is directed upward so that the exit flow reaches the slag layer and any of the remaining inclusion particles that escape being trapped by the channel have an opportunity to react with the slag and be removed there as in the case for the standard float-out method of inclusion removal.

Two important geometric parameters for the channel design/optimization study are the channel spacing, h, and the zigzag angle, θ, as shown in Fig. 2. The study was performed through numerical simulation of the steel flow through the channel with the calculation of the particle trajectories for various combinations of these basic geometric parameters. Results were compared and analyzed and an optimum pair of these parameters was determined for the channel design which was used later in the three-dimensional simulation of the actual industrial tundish.

In the flow simulation, no-slip boundary conditions were used at the channel walls and constant pressure conditions were specified at the outlet. The inlet velocity components were derived/extracted from the three-dimensional tundish (without the zigzag channels) flow simulation at the location where the channel insert was to be placed. A systematic grid refinement study was conducted to obtain the optimum mesh distribution. The nodes were clustered towards the channel walls. Four different channel spacings, 0.0127, 0.0254, 0.0381, and 0.0508 m (0.5, 1, 1.5, and 2 in.), and four different zigzag angles (30˚, 45˚, 60˚, and 70˚) were considered resulting in a total of 16 different simulations.

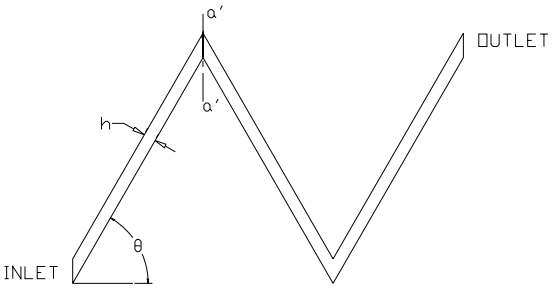

Figure 2: Schematic diagram of the two-dimensional zigzag channel.

The flow streamlines for each of the 16 channel configurations are shown in Fig. 3 where it is observed that the flow recirculation occurs at the vertices of the zigzag channel and on the opposite walls immediately downstream of the vertices. The extent of the recirculation regions in the domain increases with increasing passage width for each particular zigzag angle. Excessive recirculation within the channel will be detrimental to the objective of bringing the particles into contact with the channel surfaces. A representative estimate of the percent recirculation volumes compared to the total volume within the channel with a 0.0254 m (1 in) spacing for various zigzag angles is presented in Table 1. The estimate was completed by plotting the streamlines on a fine graph paper and counting the number of small squares encircled by the recirculation bubbles. From these results it is noticed that while the recirculation volume is a maximum for the 45˚ angle, it is similar to that for the 60˚ and 70˚ zigzag angles.

For the optimum channel design, the pressure drop across the channel must not be excessive. The pressure drop, as a function of the zigzag angle, θ, is presented for various passage spacings in Fig. 4. While the pressure drop is not strongly affected by the passage spacing; it increases significantly with the zigzag angle. The pressure drop beyond a 60˚ zigzag angle seems to be excessive.

The most important feature to consider for the design of the zigzag channel to fulfill the objective of this research is the particle trajectory history

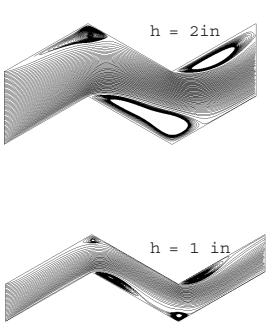

Figure 3a: Streamlines in the zigzag channel, θ =30˚.

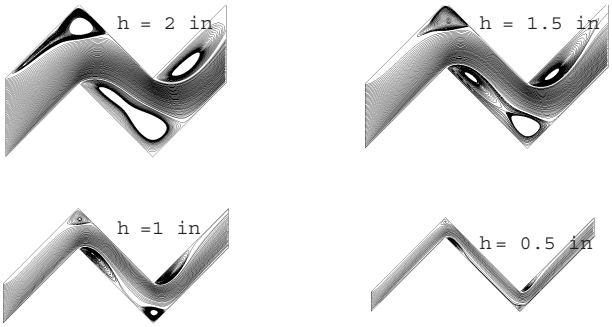

Figure 3b: θ =45˚.

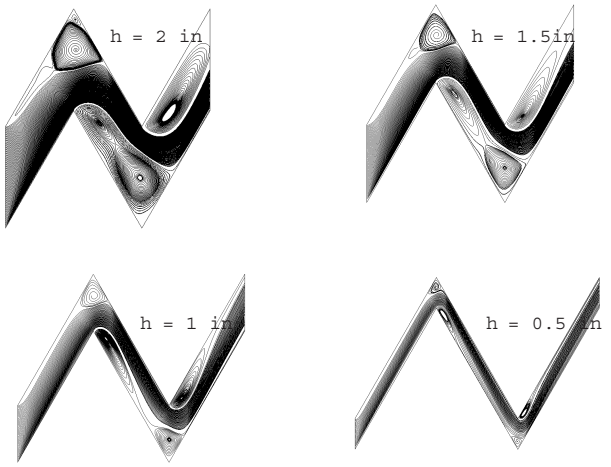

Figure 3c: θ =60˚.

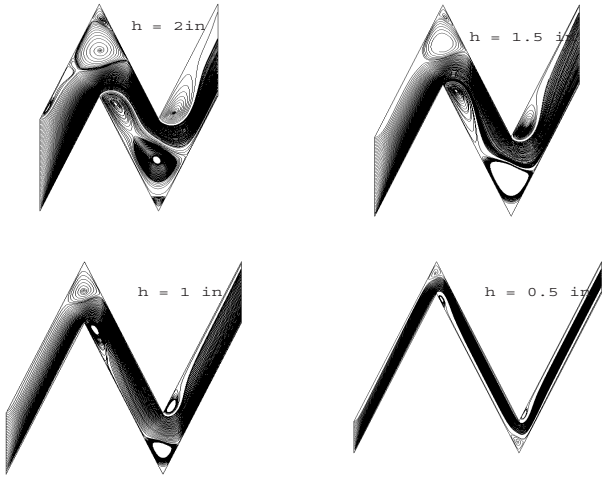

Figure 3d: θ =70˚.

through the channel. To this effect the trajectories of particles inside the channel were determined by applying the particle dynamics equation [Eq. (7)]. The particle trajectories for a channel with a 0.0254 m (1 in) spacing and 60˚ angle are shown in Fig. 5. To understand the effects of the particle size on the trajectories, the diameter of the particles were varied as 25, 50, 75, and 100 μm. Particle trajectories depend upon the flow field in the zigzag channel and the various forces including the buoyancy force exerted on the particle. In general, larger particles tend to rise to the top surface of the channel near the inlet section which is desirable for the objective. This can be directly attributed to the larger buoyancy force exerted on the larger size particles. Smaller particles, experiencing lesser buoyancy force, tend to flow along with the fluid and then exit through the channel outlet. However, many smaller particles impact the channel wall especially on the second inclined top surface and the third inclined bottom surface during their travel through the zigzag channel.

Table 1: Recirculation volume estimates in percent of total channel volume for a channel with 1 inch spacing.

Zigzag angle	Percent recirculation volume
30˚	7.65
45˚	20.14
60˚	16.23
70˚	16.31

Considering the effects of various geometric parameters such as the zigzag angle and passage spacing and fluid dynamic factors such as the recirculation volume, particle behavior, and pressure drop across the channel, a channel having

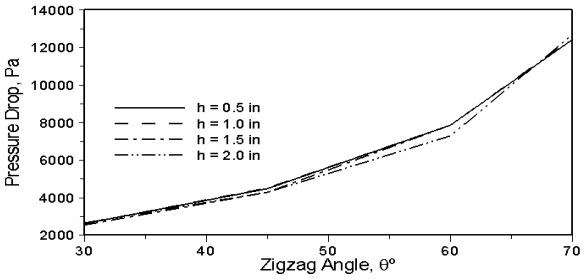

Figure 4: Pressure drop across the channel.

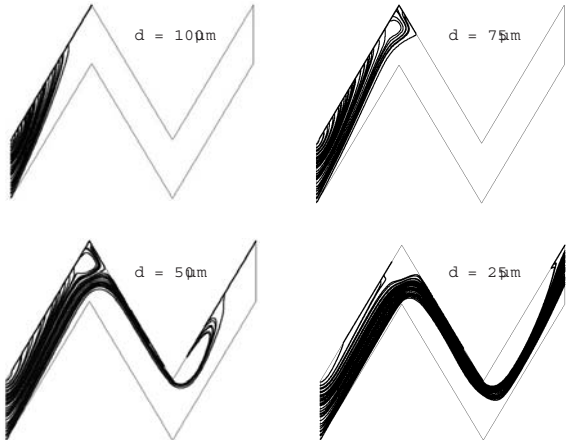

Figure 5: Particle trajectories in the zigzag channel with 1 inch spacing and 60˚ angle.

a zigzag angle of 60˚ with a passage spacing of about 0.0254 m (1 in) is a near optimum channel design for effective chemical trapping of the inclusions. As such, this configuration of the zigzag channel was recommended for implementation in the complete three-dimensional model of the tundish flow simulation.

3.2 Three-dimensional tundish

Two different numerical models; one of the existing tundish and the other of the tundish with the zigzag channel block in place, were considered. The hydrodynamic field in the existing tundish was first calculated and analyzed to understand the overall tundish flow behavior and to identify a strategic location for the placement of the zigzag channel block within the tundish.

The unstructured tetrahedral meshes for both models, as shown in Fig. 6, were generated by the mesh generation module of the CFD-ACE+^{TM} code. A dense mesh was employed near to the inlet shroud, within the pour pad, near to the outlet nozzles, and near all of the walls of the tundish. The intense computational demand of these did not allow a systematic grid refinement study to be performed. However, after few preliminary trials, a mesh with ∼150,000 cells was deemed satisfactory for the feasibility study as the quantitative accuracy was not a major concern at this point.

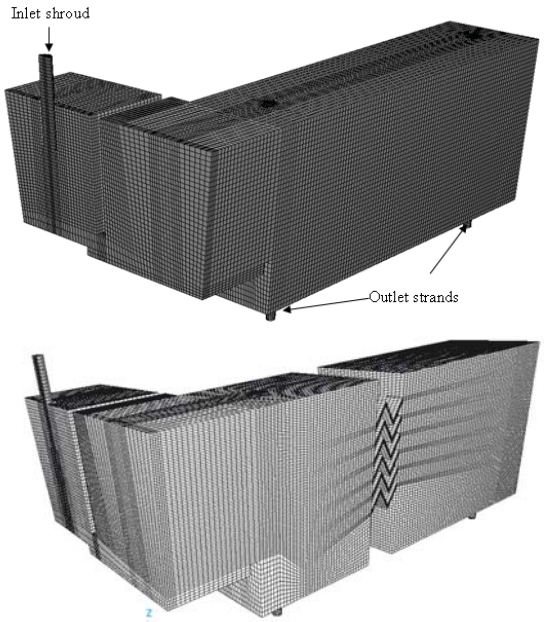

Figure 6: Mesh for tundish models; top –without the zigzag channel, bottom– with the zigzag channel block.

A uniform volumetric flow rate of 0.00355 m^3/s obtained from real tundish data was specified at the inlet. This translated to a uniform inlet velocity of 0.628 m/s downward with an inlet Reynolds number of ∼40,000. Constant pressure (0.0 Pa) conditions were specified at the outlet. No-slip conditions were imposed at all of the walls except for the top surface and the symmetry plane where zero shear stress and zero normal velocity conditions were imposed (Ilegbusi and Szekely, 1987). Isothermal conditions were assumed and as such it was not necessary to solve the energy equation.

3.2.1 Tundish flow without the zigzag channel insert

Within the pour pad chamber of the tundish, which is contained by the weir, the fluid jet from the inlet shroud impinges on the bottom, spreads outward radially, bounces back ascending near to the chamber walls, hits the top surface, goes down again, and ultimately exits the pour pad chamber through the opening beneath the weir. This produces a vigorous turbulent intermixing of the fluid and inclusion particles within the inlet chamber. This is depicted by the streamtrace plots within the pour pad chamber using mass less particles of negligible diameter released at the inlet. This pattern is shown in Fig. 7.

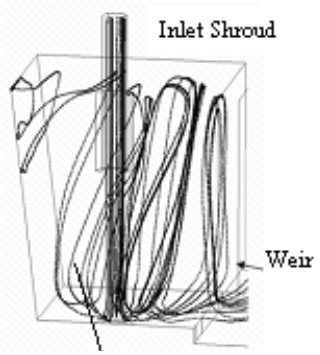

Figure 7: Streamtrace plots within the pour pad.

The overall flow pattern throughout the tundish can be visualized in the sample streamtrace plots presented in Fig. 8. A strong helical form of motion of the fluid before its entry into the main tundish chamber is noticeable. In the main tundish cavity, however, the flow does not appear quite as erratic as it is in the inlet zone. This is because of the large reduction of the flow velocity magnitude.

As expected, the geometry of the tundish furniture has a profound influence on the flow behavior of the molten steel within the tundish. The purpose of the small span-wise dam at the entry to the main tundish cavity is to prevent the molten steel from going directly to the outlet nozzles and short-circuiting the overall flow pattern. This is clearly depicted by the streamtrace plots shown in

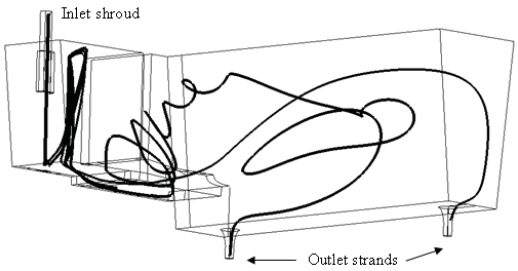

Figure 8: Streamtraces depicting the flow from the inlet shroud to the outlet nozzles.

Fig. 9. The dam also guides the flow upwards which has two purposes. First, it increases the residence time and second, the steel flow comes into contact with the slag layer where the inclusion particles are able to react and coagulate with the slag, thereby reducing the inclusion particle content to some extent.

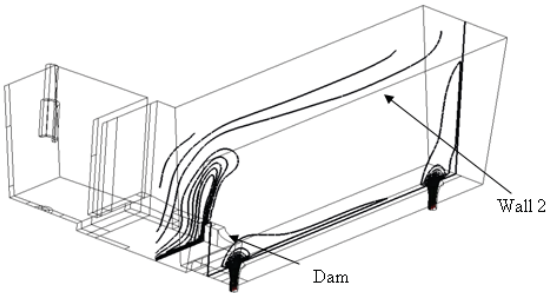

Figure 9: Streamtraces depicting the flow over the small dam.

The turbulence level in the fluid stream is a quantity of interest here. A contour plot of the kinetic energy of turbulence on a vertical *xz* plane through the tundish cavity is presented in Fig. 10. It shows large gradients and peaks at the entry region to the main tundish cavity and again in the vicinity of the outlet area.

3.2.2 Tundish with a zigzag channel insert

Because of the presence of the zigzag channel block, the main tundish cavity is conveniently divided into two chambers between which the chan-

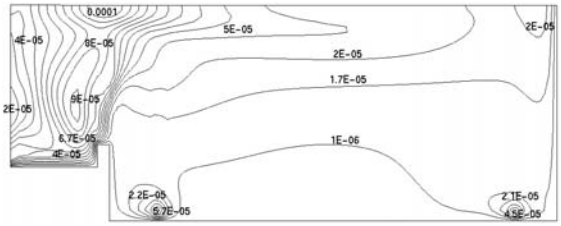

Figure 10: Contours of the turbulent kinetic energy (m^2/s^2) on a *xz* plane through the tundish cavity.

nel block acts as a flow barrier. Pre-simulation suspicions were that this might severely reduce the flow through the downstream outlet nozzle near the end wall. This, however, does not happen as the flow through the downstream outlet is reduced only by about 5%. A streamtrace plot through the tundish is shown in Fig. 11. This shows the flow pattern differences in the tundish compared to that in Fig. 8 which is for the same tundish without the zigzag channel. Erratic motion in the entry region and a large recirculation zone occurs in the second portion of the main tundish cavity downstream of the zigzag channel block.

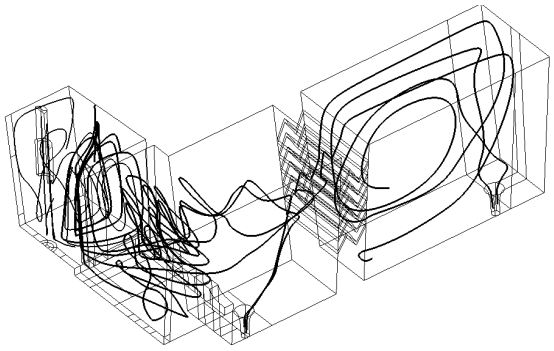

Figure 11: Streamtraces in the tundish with the zigzag channel.

A sample plot of the turbulent kinetic energy for the same *xz* plane as in Fig 10 is shown in Fig. 12. Very large gradients of the turbulent kinetic energy upstream bottom part of the dam, top of the dam, near the outlets, and on the upstream side of the zigzag channel block is noticeable. The turbulence intensity distribution is sigficantly different from that in Fig 10 for the case of the tundish without the zigzag channel block.

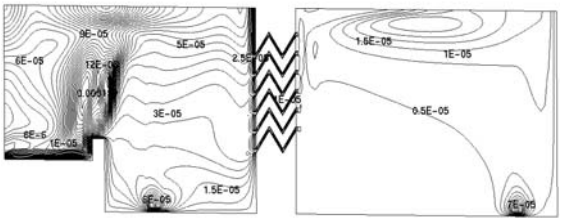

Figure 12: Contours of the turbulent kinetic energy (m^2/s^2) on a *xz* plane through the tundish cavity.

3.2.3 Particle trajectories in the tundish with the zigzag channel

Computation and visualization of the particle trajectories in the tundish equipped with the zigzag channel block is the most important aspect of this study since that will determine the ultimate feasibility of the inclusion trapping and filtering technique. For that reason extensive computation of the particle trajectories and their critical visualization were performed. Initially, the coefficient of restitution for the particle to zigzag channel wall collision was set to 1 for which case the particles bounce back from the wall with the same speed as before the wall collision, as mentioned in section 2.3. Particles having uniform diameters were released at the inlet and the trajectories were computed as they passed through the flow domain. The trajectories for 100 μm and 75 μm diameter particles are depicted in Figs. 13 and 14. Very erratic and irregular motion of the particles in the entry region and in the main tundish cavity upstream of the zigzag channel is evident. This is because of the erratic motion of the fluid phase (the molten steel) in those regions. In the portion of the cavity downstream from the zigzag channel, the larger particles (100 μm) have relatively smooth trajectories (Fig. 13) compared with the smaller (75 μm) particles (Fig. 14). Trajecto-

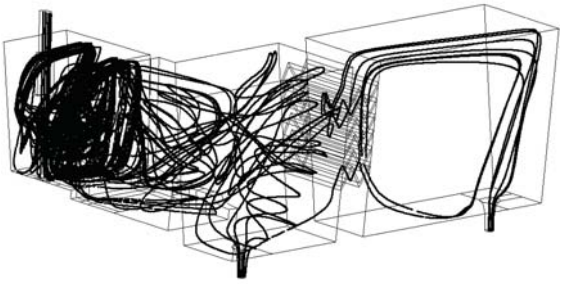

Figure 13: Trajectories of 100 μm diameter particles when the coefficient restitution for wall collision is set to 1.

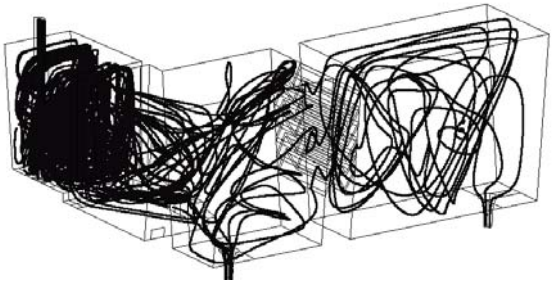

Figure 14: Trajectories of 75 μm diameter particles when the coefficient restitution for wall collision is set to 1.

ries for a distribution of particles of various diameters (1-100 μm) released at the inlet are shown in Fig. 15. It has the same general trend as Figs. 13 and 14. The same situations are repeated with the coefficient of restitution for the particles to the zigzag channel wall collision set equal to zero. This mimics total particle adsorption at the wall in an *ad-hoc* manner. The particle trajectories for this case are shown in Fig. 16. It can be seen that none of the particles pass through the zigzag channel block into the downstream portion of the cavity. This is quite remarkable in the sense that it demonstrates, albeit in a simulated fashion, the effectiveness of the zigzag channel surface in trapping the inclusion particles. It is thus expected that the proposed filtering technique has the potential to be successful. It will depend on the capture efficiency of the zigzag channel trap.

The next step in this research is to actually fab-

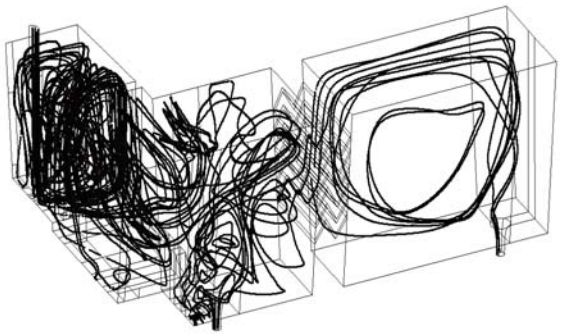

Figure 15: Trajectories of 1-100 μm diameter particles when the coefficient restitution for wall collision is set to 1.

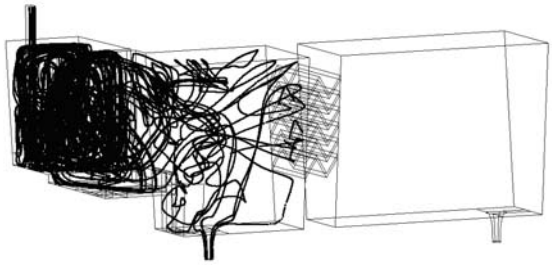

Figure 16: Trajectories of 1-100 μm diameter particles when the coefficient restitution for wall collision is set to 0.

ricate the zigzag channel block and install it in an existing tundish and conduct field trials. This phase is currently underway. It is anticipated that because of the adhesion of the inclusion particles to the zigzag channel surfaces, the channels will become somewhat clogged and the channel block will have to be replaced periodically. The time when the channels will be clogged beyond their usable condition and how frequently they have to be replaced will depend on the capture rate of the inclusions by the zigzag channel trap. It will not be known until the field trials are conducted. Further optimization of the channel block design may be required based on the field trial results. The results of the field testing and subsequent channel design optimization will be reported in a subsequent paper.

4 Summary and Conclusions

A physical-chemical filtering system for the removal of inclusion particles from molten steel in the tundish has been proposed. The molten steel will be directed through zigzag channels in the tundish furniture. The inclusion particles are expected to come in contact with the zigzag channel surfaces while passing through them because of the increased recirculation and turbulence. The inclusion particles are expected to stick to the zigzag channel surfaces and bond and get trapped there. The feasibility of the filtering system has been evaluated numerically and the results are reported in this study. The flow field in the tundish was computed by solving the incompressible RANS equations employing the standard $k-\varepsilon$ turbulence model. The particle trajectories were computed by solving a Lagrangian particle dynamics equation where the particles are subjected to various physical and hydrodynamic forces. The trajectories are then visualized and critically examined to assess the effectiveness of the proposed filtering system.

Design optimization of the zigzag channel was performed by first computing the flow through a two dimensional zigzag channel and then computing the particle trajectories through the channels. A channel with 60^o zigzag angle and 0.0254 m (1 in) channel spacing was deemed satisfactory for the purpose. A channel block consisting of the same channel design was then inserted into a three-dimensional model of an existing continuous casting tundish. The hydrodynamic field and the particles trajectories in the modified tundish model were then calculated and examined. It is concluded that the proposed filtering technique will be very effective in removing the inclusion particles in the tundish. The actual physical verification of the effectiveness of the filtering system will be pursued in field tests shortly in the Timken plant.

Acknowledgement: This work is funded through the American Iron and Steel Institute's Technology Roadmap Program for the Steel Industry (AISI - TRP Project No. 9757). The sponsors are Timken Company and the US Department of Energy (DE-FC36-97ID13554).

References

Abhilash, E.; Joseph, M.A.; Krishna, P. (2006): Prediction of dendritic parameters and macro hardness variation in permanent mould casting of Al-12%Si alloys using artificial neural networks. *Fluid Dynamics & Materials Processing*, vol. 2, pp. 211-220.

Amberg, G.; Shiomi, J. (2005): Thermocapillary flow and phase change in some wide spread materials processes. *Fluid Dynamics & Materials Processing*, vol. 1, pp. 81-95.

Chakraborty, S.; Sahai, Y. (1991): Effect of varying ladle stream temperature on the melt flow and heat transfer in continuous casting tundishes. *ISIJ International*, vol. 31, pp. 960-967.

Chevrier, V.F. (2000): Droplet and bubble separation at the interface between a liquid metal and a liquid slag. Ph.D dissertation, Carnegie Mellon University.

Clift, R.; Grace, J.R.; Weber, M.E. (2005): *Bubbles, Drops, and Particles*. Dover Publications.

Dash, K.S.; Jha, K.P. (2002): Effect of outlet positions and various turbulence models on mixing in a single and multi-strand tundish. *International Journal of Numerical Methods for Heat and Fluid Flow*, vol. 12, pp. 560-584.

Dash, K.S.; Jha, K.P. (2004): Employment of different turbulence models to the design of optimum steel flows in a tundish. *International Journal of Numerical Methods for Heat and Fluid Flow*, vol. 14, pp. 953-979.

ESI-CFD (2006): CFD-ACE+^{TM} Manual published by ESI-CFD, Inc.

He, Y.; Sahai, Y. (1990): Influence of some factors on fluid flow in continuous casting tundishes. *Acta Metallurgica Sinica. B*, vol.3. pp. 49-53.

Hong, C.P.; Zhu, M.F.; Lee, S.Y. (2006): Modeling of dendritic growth in alloy solidification with melt convection. *Fluid Dynamics & Materials Processing*, vol. 2, pp. 247-260.

Ichibashi, H. (1986): Application of filter for the clean steel. Proceedings of the Fifth International

Iron and Steel Congress, Tundish Metallurgy, vol. 1, pp. 677-687

Ilegbusi, O.J.; Szekely, J. (1987): The modeling of fluid flow, tracer dispersion and inclusion behavior in tundishes. *Mathematical Modeling of Materials Processing Operations*, Szekely, J., eds., TMS, Warrendale, PA, pp. 409-429.

Itoh, H.; Hino, M.; Ban-ya, S. (1997): Thermodynamics on the formation of spinel nonmetallic inclusion in liquid steel. *Metallurgical and Material Transaction B - Process Metallurgy and Materials Processing Science*, vol. 28, pp. 953-956.

Javurak, M.; Kaufmann, B.; Gerhard, Z.; Philipp, G. (2002): Inclusion separation in tundishes - some new general aspects. *Steel Research*, vol. 73, pp. 1-7.

Launder, B.E.; Spalding, D.B. (1974): The numerical computation of turbulent flows. *Computational Methods for Applied Mechanics and Engineering*, vol. 3, pp. 269-289.

Lopez-Ramirez, S.; Morales, R.D.; Serrano, J.A.R. (2000): Numerical simulation of the effects of buoyancy forces and flow control devices on fluid flow and heat transfer phenomena of liquid steel in a tundish. *Numerical Heat Transfer Part A – Applications*, vol. 37, pp. 69-86.

Ludwig, A.; Gruber-Pretzler, M.; Wu, M.; Kuhn, A. Riedle, J. (2005): About the formation of macrosegregations during continuous casting of Sn-Bronze. *Fluid Dynamics & Materials Processing*, vol. 1, pp. 285-300.

Lun, C.K.K.; Liu H.S.,(1997): Numerical simulation of dilute turbulent gas-solid flows in horizontal channels. *International Journal of Multiphase Flow*, vol. 23, pp. 575-605.

Narski J. and Picasso M., (2007): Adaptive 3D finite elements with high aspect ratio for dendritic growth of a binary alloy including fluid flow induced by shrinkage, *FDMP: Fluid Dynamics & Materials Processing*, Vol. 3, No. 1, pp. 49-64

Patankar, S.V. (1980): *Numerical Heat Transfer and Fluid Flow*. Hemisphere, New York.

Ran, J.; Zhang, L.; Tang, Q.; Xin, M. (2006): Numerical simulation of the particle motion characteristics in boundary layer gas solid rotary flow. *Journal of Fluids Engineering*, vol. 128, pp. 596-601.

Saffman, P.G. (1965): The lift on a small sphere in a slow shear flow. *Journal of Fluid Mechanics*, vol. 22, pp. 385-400. Corrigendum (1968). *Journal of Fluid Mechanics*, vol. 31, pp. 624.

Schwarze, R.; Bbermeier, F.; Janke, D. (2001): Numerical simulation of fluid flow and disperse phase behavior in continuous casting tundishes. *Modeling and Simulation in Material Science and Engineering*, vol. 9, pp. 297-287.

Shen, F.; Khodadadi, J.M.; Pien, S.J.; Lan, X.K. (1994): Mathematical and Physical modeling studies of molten aluminum flow in a tundish. *Metallurgical and Materials Transaction B - Process Metallurgy and Materials Processing Science*, vol. 25, pp. 669-680.

Sheng, D.Y.; Jonsson, L. (1999): Investigation of transient fluid flow and heat transfer in a continuos casting tundish by numerical anlysis verified with nonisothermal water model experiments. *Metallurgical and Materials Transaction B - Process Metallurgy and Materials Processing Science*, vol. 30, pp. 979-985.

Taniguchi, S.; Brimacombe, J.K. (1997): Application of pinch force to the separation of inclusion particles from liquid steel. *ISIJ International*, vol. 34, pp. 722 -731.

Vargas-Zamora, A.; Morales, R.D.; Diaz-Cruz, M.; Palafox-Ramos, J.; Demedices, L.G. (2003): Heat and mass transfer of a convective-stratified flow in a trough type tundish. *International Journal of Heat and Mass Transfer*, vol. 46, pp. 3029-3039.

Yamada, W.; Kiyose, A.; Fukuda, J.; Tanaka, H.; Nakashima, J.I.. (2003): Simulation of coagulation of noon metallic inclusions in tundish and their trappings into the solidified shells in continuous casting mould. *Iron Making and Steelmaking*, vol. 30, pp. 151-157.